The Meteoritical Society

Meteoritics & Planetary Science 50, Nr 7, 1228–1243 (2015)
doi: 10.1111/maps.12466

Melting and cataclastic features in shatter cones in basalt from the Vista Alegre impact structure, Brazil

Lidia PITTARELLO[1,2*], Fabrizio NESTOLA[3], Cecilia VITI[4], Alvaro Penteado CRÓSTA[5], and Christian KOEBERL[1,6]

[1]Department of Lithospheric Research, University of Vienna, Althanstrasse 14, A-1090 Vienna, Austria
[2] Present Address: Earth System Science, Vrije Universiteit Brussel, Pleinlaan 2, B-1050 Brussels, Belgium
[3]Department of Geosciences, University of Padova, via Gradenigo 6, I-35131 Padova, Italy
[4]Department of Physics, Earth and Environmental Sciences, University of Siena, Via Laterina 8, I- 53100 Siena, Italy
[5]Institute of Geosciences, Unicamp, R. João Pandiá Calógeras 51, 13083-970 Campinas SP, Brazil
[6]Natural History Museum, Burgring 7, A-1010, Vienna, Austria
[*]Corresponding author. E-mail: lidia.pittarello@vub.ac.be

(Received 04 February 2014; revision accepted 03 April 2015)

Abstract–Shatter cones are one of the most widely recognized pieces of evidence for meteorite impact events on Earth, but the process responsible for their formation is still debated. Evidence of melting on shatter cone surfaces has been rarely reported in the literature from terrestrial impact craters but has been recently observed in impact experiments. Although several models for shatter cones formation have been proposed, so far, no one can explain all the observed features. Shatter cones' from the Vista Alegre impact structure, Brazil, formed in fine-grained basalt of the Jurassic-Cretaceous Serra Geral Formation (Paraná large igneous province). A continuous quenched melt film, consisting of a crystalline phase, mica, and amorphous material, decorates the striated surface. Ultracataclasites, containing subrounded pyroxene clasts in an ultrafine-grained matrix, occur subparallel to the striated surface. Several techniques were applied to characterize the crystalline phase in the melt, including Raman spectroscopy and transmission electron microscopy. Results are not consistent with any known mineral, but they do suggest a possible rare or new type of clinopyroxene. This peculiar evidence of melting and cataclasis in relation with shatter cone surfaces is interpreted as the result of tensile fracturing at the tip of a fast propagating shock-induced rupture, which led to the formation of shatter cones at the tail of the shock front, likely during the early stage of the impact events.

INTRODUCTION

Shatter cones consist of multiple sets of penetrative striated conical fractures that preferentially (but not exclusively) form in fine-grained rocks as result of a meteorite impact event, according to the definition by Dietz (1947, 1960). They can occur individually or in clusters of hierarchically related, roughly conical structures. As similar features cannot be produced by any other terrestrial geological process, shatter cones are considered to be the only macroscopic evidence of an impact event (e.g., French and Koeberl [2010] and references therein). Nevertheless, the process that generates these features is still debated. Shatter cones are generally considered to have formed under low shock pressure (e.g., experiments by Schneider and Wagner 1976), but cases of high shock pressure (up to ca. 25 GPa) have been reported, as suggested by the occurrence of planar deformation features (PDF) in quartz grains across the shatter cone (Hargraves and White 1996; Ferriere and Osinski 2010; Ferriere et al. 2010; Vasconcelos et al. 2013). Hypotheses on shatter cone formation include the following.

1. Scattering of shock waves due to the presence of heterogeneities in the target rock, proposed by Baratoux and Melosh (2003). This numerical model

© The Meteoritical Society, 2015.

shows that the presence of heterogeneities trigger a local increase in the tensional stress at the tail of a shock wave, by interaction with the shock waves, and results in curved fractures. The necessary conditions for the formation of shatter cones, according to this model, are (a) the shock wave must travel faster (at least by a factor of two) in the rock than in the heterogeneity, (b) the size of the heterogeneity must be comparable to the width of the shock wave, and (c) the shock pressure is assumed to be relatively low (3–6 GPa). The width of the compressive pulse and the size of the heterogeneity control the conical shape of shatter cones.

2. Tensile fractures that form only for ruptures propagating at the speed close to that of the Rayleigh waves, proposed by Sagy et al. (2002, 2004) and based on principles of fracture mechanics. Shock-wave propagation generates large tensile stresses normal to the main compressive direction. Shatter cones are formed as dynamic fractures, which are related to the tensile stresses that develop at the tail of the shock wave, and which undergo spontaneous branching at high velocity of propagation (0.9–0.98 of Rayleigh waves). The high velocity is also responsible for the spoon shape of shatter cones. The striations are due to the interaction between the fracture front and rock heterogeneities. The aperture angle of the striation depends on the distance from the impact center and is related to the relative speed of rupture propagation. The shear component is considered negligible in this model.
3. Adiabatic shear banding resulting from extreme heating localized on planes that experience the maximum shear stress during shock compression, suggested by Dawson (2009). Adiabatic shear bands form at high strain rate, as a consequence of thermal softening. Numerical modeling under low shock pressure (5 GPa) supports this hypothesis (Dawson 2009). The presence of a weak heterogeneity is necessary for initiating the cone-shaped shear band. Assuming a wide shock front, two cones with the apexes pointing to opposite directions but along the same axis were obtained.

The first two hypotheses are based on tensile failure of rock during shock pressure release, whereas the latter proposes shear failure during shock compression. The presence of heterogeneities in the target is assumed in all the considered models. Wieland et al. (2006) discussed the existing models in the context of new field evidence from the Vredefort structure and concluded that none of the above-mentioned models can explain all the features observed in the field. These authors suggested that shatter cones form by decompression, immediately after the passage of the shock wave.

The occurrence of melt decorating the shatter cone surface might provide hints for understanding the shatter cone formation process. The occurrence of melt on shatter cone surfaces reported in the literature from terrestrial impact structures shows similar features, such as (1) melt occurs at the surface of shatter cones formed in large structures, such as the Vredefort in South Africa and the Sudbury in Canada, (2) the target rock is quartz-bearing and has high silica content, and (3) the melt occurrence is described as microspherules of silica within striations (Gay 1976; Gay et al. 1978; Gibson and Spray 1998). Martini (1991) reported a kind of pseudotachylite (melt) vein on the surface of shatter cones from the Vredefort. Nicolaysen and Reimold (1999) confirmed the presence of a melt film on some samples of shatter cones from the same structure. Melt veinlets associated with shatter cones were reported, but not yet fully characterized and confirmed, in the Santa Fe structure, New Mexico (Fackelmann et al. 2008). The recent report of silica melt film on a shatter cone surface from the Keurusselkä structure, Finland, represents a qualitatively different finding because the impact structure is relatively small (27–30 km in diameter; Hasch et al. 2015). Recently, thin melt films of vesicular material have also been reported from the surface of experimentally produced shatter cones in sandstone (Kenkmann et al. 2012; Wilk and Kenkmann 2015).

The current hypotheses for melt formation on shatter cone surfaces are (1) heating and vaporization of the surface due to a combination of friction and shock, followed by condensation of the vaporized material (Gibson and Spray 1998); (2) pressure drop with a small degree of frictional heating (Wieland et al. 2006); (3) localized heating due to maximum shear stress (Dawson 2009). Hasch et al. (2015) suggested that the formation of shatter cones is related to local shock pressure excursions due to the occurrence of preexisting joints, which were also locally reactivated as fault planes, therefore supporting model 2 as described above.

Here we present a detailed study of shatter cones in basalt and, in particular, we focus on the melt that occurs along the striated surface and on ultracataclasites that develop subparallel to the striated surface. These shatter cones formed in the Vista Alegre impact structure, Brazil, in the basalt of the Serra Geral Formation. As the Vista Alegre impact structure is relatively small (9.5 km in diameter) and the target rock mostly consists of basalt, the finding of a melt film on shatter cones' surface is unusual compared with previous occurrences of melt on shatter cone surfaces described in the literature, all of which concern large

impact structures (except the Keurusselkä) that formed in silica-bearing target rocks.

GEOLOGICAL SETTING AND SAMPLE DESCRIPTION

The Vista Alegre structure, Brazil, is a 9.5 km diameter circular depression centered at 25°57′S and 52°41′W and formed in the basalts of the Paraná Basin (Fig. 1a). The Vista Alegre structure has been recently confirmed as a meteorite impact structure by the finding of shatter cones in basalts and by documentation of planar deformation features in a shocked fragment of quartz sandstone (Crósta et al. 2004, 2010). Although the impact has mainly involved the volcanic rocks of the Jurassic-Cretaceous Serra Geral Formation, shock features were also found in an eolian sandstone, which might belong either to the Upper Triassic/Lower Jurassic Piramboia Formation or the Early Jurassic to Early Cretaceous Botucatu Formations and which generally lies 700–800 m below the surface. The shocked sandstone occurs either in blocks in the central area of the depression, suggesting the presence of a central uplift (Fig. 1b), or as clasts in the impact breccia. The Serra Geral Formation consists mostly of tholeiitic basalts, with minor amounts of intermediate to acidic volcanic rocks. The circular depression, which corresponds to the current surface of the crater, is largely filled by polymict breccia (Fig. 1b), which contains fragments of igneous and, in minor amounts, sedimentary rocks. This impact breccia can be considered a suevite (according to the terminology defined in Stöffler and Grieve 2007), because impact melt particles have been found in it (Crósta et al. 2012).

A quarry next to the village of Vista Alegre (Fig. 1b), located at 25°56′07 S and 52°42′21 W, provides the best exposure of the polymict breccia that fills the crater. This breccia appears grayish in color on fresh surfaces and consists of angular lithic clasts, ranging in size from mm to tens of cm, suspended in a fine-grained (pelitic) clastic matrix (Crósta et al. 2010). The clasts are mostly of igneous rocks, belonging to the Serra Geral Formation, but also a few fragments of sandstone are present. Some of the clasts have a dark, homogenous appearance and rounded forms, suggesting the occurrence of impact melt (Crósta et al. 2012). Locally the igneous clasts reveal striated surfaces when broken interpreted as shatter cones, which were believed to have deposited together with the breccia. Shatter cones occur within the polymict breccia in nest shape or as individual cones, with a size ranging from 0.5 to 20 cm (Fig. 2). Shatter cones formed in fine-grained tholeiitic basalt, with a composition very similar to that of the unshocked basalt (Crósta et al. 2010).

METHODS

The selected sample, collected in the field by C.K. and A.P.C., was investigated in a polished thin section (35 μm thickness), which was prepared by mechanical polishing using alumina suspension. A further fine polishing was performed on an active rotary-head polisher using a colloidal silica suspension with pH 9.2–10 (Köstrosol™ 3530). A FEI Inspect S50 scanning electron microscope (SEM), equipped with an EDAX Apollo XV silicon drift detector for EDX spectrometry was used for SE- and BSE imaging and qualitative major element compositional analysis at instrument settings of 10 mm working distance (WD), 10–15 kV accelerating voltage, and varying beam current. Focused ion beam (FIB) tomography and high-resolution SE- and BSE imaging were performed using a FEI Quanta 3-D FEG instrument at the Center of Earth Sciences at the University of Vienna (Austria). This FIB-SEM is equipped with a field-emission electron source for electron microscopy at high spatial resolution and a field-emission Gallium source for site nano-milling. The instrument settings were 13 mm WD, 15 kV accelerating voltage and 2 nA beam current in analytic mode using a SEM aperture of 1 mm. The same instrument has been used also for TEM foil (90 nm thick) preparation, by sputtering with gallium ions, with an ion beam accelerating voltage of 30 kV and a beam current of 3 nA. Quantitative chemical analyses of individual phases was performed with a Cameca SX100 electron microprobe at the Department of Lithospheric Research of the University of Vienna, equipped with four wavelength-dispersive spectrometers and one energy-dispersive spectrometer, with accelerating voltage 15 kV and beam current of 20 nA. The analyses were corrected according to the standard ZAF procedure and mineral formulae were calculated manually.

Chemical compositions were determined on a sample of unshocked basalt and one shatter cone of basalt in the impact breccia, on representative aliquots weighing about 30 g each. They were crushed in polyethylene wrappers and powdered in a mechanical agate mill. Contents of major and selected minor elements were determined with a Philips PW2400 X-ray fluorescence (XRF) instrument of the University of Vienna. Details of the analytical procedures and accuracies are similar to those given in Reimold et al. (1994). The contents of some major (Na, K, and Fe) and of trace elements were determined by instrumental neutron activation analysis (INAA) at the Department of Lithospheric Research, University of Vienna. About 130 mg of powdered sample and ca. 90 mg of three international rock standards (the carbonaceous chondrite Allende, Smithsonian Institution, Washington,

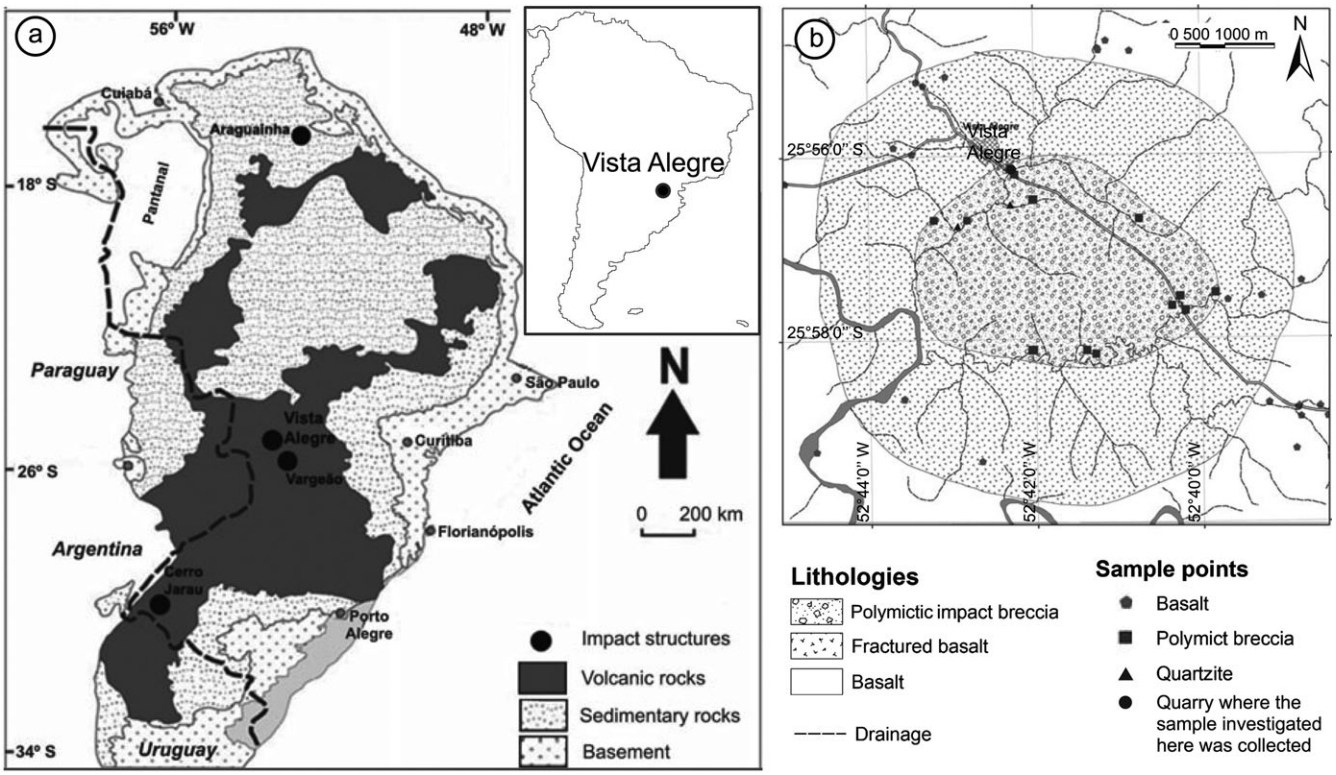

Fig. 1. Geographical, geological, and topographical setting of the Vista Alegre impact structure. a) Extension of the volcanic terrains of the Serra Geral Formation in the area. Other impact structures are indicated, such as Vargeão and Cerro do Jarau (the latter not yet confirmed) also excavated in the basalts of the Paraná Basin, and Araguainha. Map after Crósta et al. (2010). b) Schematic geological map of the crater area, modified after Crósta et al. (2010).

D.C., USA, Jarosewich et al. 1987; the Ailsa Craig Granite AC-E, Centre de Recherche Petrographique et Geochimique, Nancy, France, Govindaraju 1989; and the Devonian Ohio Shale SDO-1, United States Geological Survey, Govindaraju 1989) were sealed in polyethylene capsules and irradiated in the 250 kW Triga Mark-II reactor at the Atomic Institute of the Austrian Universities. More details on the instrumentations, method, and accuracy are given by Koeberl (1993) and Mader and Koeberl (2009). Results for those elements measured by both techniques yielded comparable values (relative standard deviation mostly below 1% for most of these elements). For some trace elements (e.g., Ir), only upper limits can be reported.

Raman spectroscopy has been performed at the Vrije Universiteit Brussel with a confocal Raman microscope LabRAM HR Evolution (HORIBA Scientific), equipped with a multichannel air-cooled CCD detector (spectral resolution <1 cm^{-1}, lateral resolution 0.5 μm, axial resolution 2 μm) and using a solid-state laser corresponding to green light (532 nm), with beam current of 2.5 mW. Transmission electron microscopy (TEM) was performed at the Department of Physics, Earth and Environmental Sciences of the University of Siena, using a JEOL 2010, with 200 kV accelerating voltage, LaB_6 electron source, ultrahigh-resolution (UHR) pole piece, and point-to-point resolution of 1.9 Å. The microscope is also equipped with an ultra-thin window Oxford ISIS energy-dispersive spectrometer, allowing chemical analyses of nanovolumes.

RESULTS

Shatter Cone

A shatter cone sample collected in the quarry indicated in Fig. 1b has been selected for this study. This sample consists of a clast of basalt in the polymict breccia, showing striations on opposite surfaces and crosscut by fractures parallel to the striated surfaces (Fig. 3a). These fractures are filled by a fine-grained cataclasite (Fig. 3b), marked by a reddish color in plane-polarized light. A melt rock film, with a glassy appearance at the optical microscope (Fig. 3c), is locally preserved along the striated surface. This glassy layer has an average thickness of ca. 50 μm.

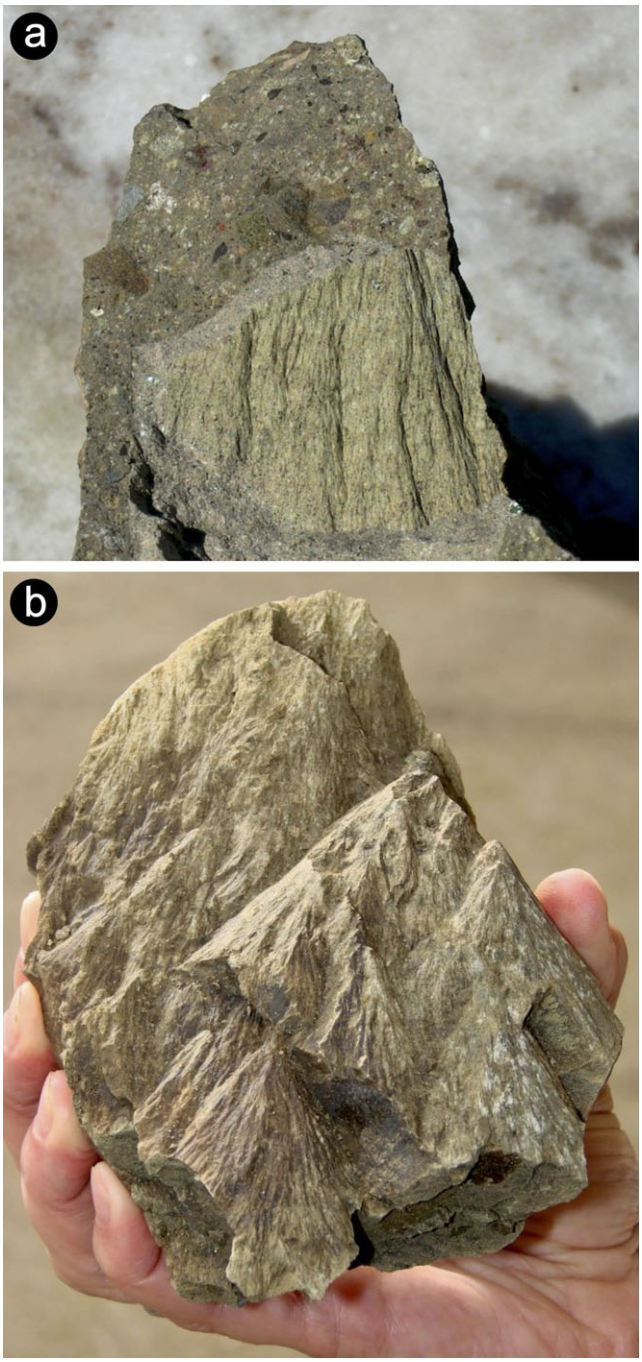

Fig. 2. Shatter cones in the polymict breccia of the Vista Alegre structure a) Individual shatter cone in the breccia. Base of the shatter cone is 5 cm. b) Cluster of shatter cones formed in basalt.

The chemical composition of a sample of unshocked basalt collected outside the crater and that of a shatter cone clast embedded in the impact breccia are compared in Table 1. The differences are consistent with the internal variability in the volcanic sequence. The only notable variation is the loss on ignition (LOI), which is much higher in the shatter cone sample than in the unshocked basalt, but is similar to that measured in the bulk impact breccia where shatter cones were found (Table 1). The basalt of the shatter cone sample consists mainly of plagioclase (An_{53}; Table 2), pyroxene (augite; Table 2), and magnetite, with grain size in the range of 50-70 μm. The oblique alignment of magnetite grains (Fig. 3d) is likely related to the basalt emplacement and shows no relations with the orientation of shatter cones striations.

Cataclasites

In the selected shatter cone sample, the cataclastic layers have an average thickness of ca. 30 μm and sharp margins with the basalt of the shatter cone (Figs. 4a and 4b). Locally, an offset is recognizable: in Fig. 4a, magnetite exhibits an uncommon shape, as if it was cut along the cataclasite. As this grain of magnetite is not visible on the other side of the cataclasite, we cannot evaluate the offset in the studied section. The cataclastic layer consists of pyroxene clasts embedded in a very fine-grained matrix (Fig. 4c). The pyroxene clasts, about 10 μm in size, have subrounded surface but are slightly elongated and are generally oriented subparallel to the cataclasite margin. The composition of pyroxene clasts can be considered consistent with that of pyroxene in the host basalt (Table 2). A rim of ultrafine-grained particles coats the clasts (Fig. 4c). The matrix has an average grain size of less than 50 nm and shows evidence of sintering and aggregation of the grains (Fig. 4d). Qualitative analyses on the matrix grains suggest a composition close to that of the pyroxene in the host, but the grain size has hampered quantitative microprobe measurements. The cataclasite is crosscut by secondary veins that locally extend in the host basalt and that are mostly filled by likely sheet minerals (Fig. 4b). >

The Melt Layer

The striated surface of the selected sample is decorated by a thin melt rock film with an average thickness of 50 μm (Fig. 5a). The melt layer has sharp margin with the host basalt (Figs. 5a and 5b). Generally, no reactions are observed between the melt and the host, except when a magnetite grain occurs. In this case, the magnetite displays effects of thermal breakdown and the melt has an embayment in the magnetite site (Fig. 5c). The melt layer is nearly completely crystallized, but a few areas between crystals might be amorphous (dark gray in BSE-SEM images; Figs. 5b–d). The crystals are acicular to dendritic in shape, locally forming star-shaped aggregates. The grain size of these crystals and aggregates is of micrometer

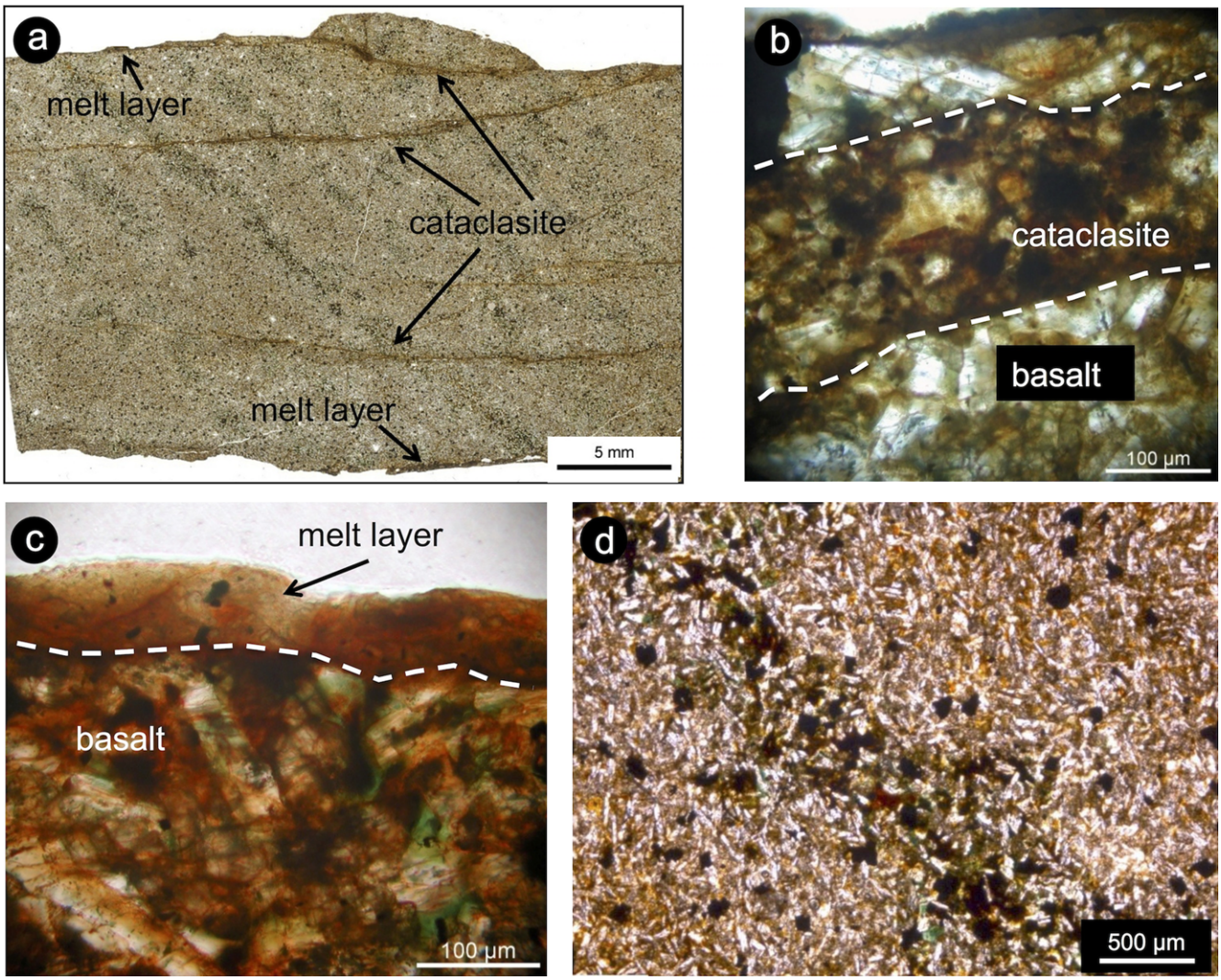

Fig. 3. Microstructures in the selected sample of shatter cone from the Vista Alegre structure. a) Scan of the thin section. The cut has been done normal to the striated surface and parallel to the striations. Striations are present both on top and bottom of the sample and the melt layer occurs on both surfaces but is more continuous on the top. Notice the occurrence of cataclastic layers parallel to the striated surface, marked by incipient alteration, and the oblique layering consisting of concentration of Fe-oxides. b) Detail of the cataclastic layer. c) Detail of the melt layer along striation. d) Detail of the layering of Fe-oxides in the basalt. Plane-polarized light photographs.

scale (Figs. 5b and 5d) and seems to decrease slightly from the center of the layer toward the margin.

Micrometer-sized crystals in the melt layer have been investigated by electron microprobe analysis. Due to the fine grain size of the crystals and the possible intergrowth with other material in comparison with the interaction volume of the microprobe, only two analyses among many were considered representative of the investigated phase (Table 2). These analyses show the smallest standard deviation and the largest total in wt%, above 95%, and therefore suggest the least contamination by the neighboring phases. The obtained composition is mixed between plagioclase and pyroxene. In fact, transmission electron microscopy revealed that the melt layer consists of a fine/ultrafine association of three different phases, i.e., (1) nanocrystals of an unidentified phase; (2) "bridges" of phyllosilicates; and (3) an amorphous matrix, likely glass (Fig. 6). The unidentified nanocrystals have grains size up to 1 µm, with subrounded to elongated shape. Locally, crystals display hypidiomorphic shapes, but generally the grain boundaries are irregular and show embayments filled by amorphous material. These nanocrystals do not exhibit any internal strain contrast features. The diffraction pattern allows estimation of possible cell parameters, which are consistent with either orthorhombic or

Table 1. XRF and INAA analyses of selected samples from the Vista Alegre impact structure.

	Serra Geral basalt	Shatter cone clast	Bulk impact breccia
SiO_2	51.55	48.38	49.97
TiO_2	1.82	1.51	1.56
Al_2O_3	12.46	9.96	12.58
Fe_2O_3	15.73	14.68	12.63
MnO	0.26	0.21	0.18
MgO	3.82	8.05	4.44
CaO	7.86	9.66	8.11
Na_2O	2.86	1.56	2.75
K_2O	1.38	0.32	1.23
P_2O_5	0.22	0.14	0.21
LOI	0.69	4.66	5.29
Total	98.65	99.13	98.91
Sc	39.1	46.2	34.5
V*	550	348	349
Cr	36.6	284	60.4
Co	44.0	50.4	38.2
Ni*	31.9	95.6	37.0
Cu*	160	162	157
Zn*	109	101	93.1
As	<2.4	<1.3	0.70
Se	<1.8	<3.1	<2.2
Br	<0.3	<0.2	<0.2
Rb*	49.6	5.2	40.4
Sr*	185	260	280
Y*	96.9	30.7	33.1
Zr*	155	79.2	136
Nb*	9.3	3.4	9.0
Sb	<0.2	<0.2	<0.2
Cs	1.36	0.34	1.58
Ba*	297	23.2	244
La	30.4	6.03	17.6
Ce	38.0	13.6	34.8
Nd	28.7	9.78	18.7
Sm	8.24	3.42	5.28
Eu	2.53	1.09	1.50
Gd	11.1	3.49	5.30
Tb	1.64	0.72	0.90
Tm	0.88	0.42	0.48
Yb	6.12	2.44	2.86
Lu	0.96	0.39	0.44
Hf	4.15	2.16	3.53
Ta	0.58	0.18	0.70
Ir (ppb)	<2.1	<4.0	<2.9
Au (ppb)	1.57	<1.4	<1.4
Pb*	9.2	3.2	7.3
Th	4.59	0.96	4.33
U	<0.6	<0.5	0.91

Major elements in wt%, trace elements in ppm, except as noted. The contents of all the major elements and the minor elements marked with * were measured by XRF; the remaining minor and trace element abundances were measured using INAA. All Fe is reported as Fe_2O_3.

monoclinic symmetry classes (Fig. 7). The EDX analyses on this phase, at high analytical resolution, have confirmed the microprobe quantitative analyses (Table 2). Selected EDX analyses of the mica and of the amorphous material are also listed in Table 2.

In summary, cataclastic layers and the melt film have some features in common (1) sharp margins with the host rock, (2) subparallel orientations with respect to the striated surface of shatter cones, (3) comparable and constant thicknesses (30–50 μm), and (4) ultrafine-grained crystals in the groundmass. Differences are (1) cataclasites locally show offsets, not observed for the melt film, (2) magnetite at the margin of the melt film displays thermal breakdown, (3) pyroxene clasts in the cataclasite have subrounded shapes, and (4) in the melt film phases have crystallized with skeletal shapes.

DISCUSSION

Comparison with Previous Findings of Melt and Related Features in Shatter Cones

Melt decorating shatter cone surfaces has been previously reported in only a few confirmed impact structures so far (Wieland et al. [2006] and references therein). A possible further structure, Keurusselkä, exhibiting melt layers on shatter cones surfaces could be added to list (Hasch et al. [2015] and references therein). A few publications provide detailed investigations of this melt. Nicolaysen and Reimold (1999) described a thin (maximum 500 μm) glassy layer decorating highly oxidized surface of shatter cones in quartzite from the Vredefort impact structure. Similar layers crosscut the quartzite, with subparallel orientations with respect to the striated surface and locally showing small offsets. These features are quite similar to our findings in Vista Alegre shatter cones, except for the composition. The shatter cones studied by Nicolaysen and Reimold formed in quartzite and, therefore, the melt consists of pure SiO_2 or a mixture of SiO_2 and Al_2O_3. The authors also found glass spherules on the striated surface, similarly to the observations by Gay et al. (1978), and related their formation to frictional slip. Unfortunately no further investigations on the melt layers and on the possible crystalline phases were performed. Gibson and Spray (1998) described melt occurrences on shatter cone surfaces from the Sudbury impact crater. On the striated surface, the authors found smears and fibers, up to 50 μm in length, which are stretched along the striation, locally stretched up to beyond their elastic limit and are, therefore, broken. Even microspherules, similar to those described from the Vredefort shatter

Table 2. Composition of the investigated phases. The analyses were made using the electron microprobe, but EDX analyses collected with the TEM are also shown, because the high analytical resolution of the technique allows extremely well-focused semiquantitative analyses on submicrometer-sized phases.

	Basalt		Cc	Melt layer	EDX (TEM)		
	Plg	Px	Px clast	UM (avg #2)	UM (avg #15)	Mica	am.ph
Na_2O	5.03	0.19	0.22	2.99 ± 0.01	3.58 ± 0.26	0.39	0.71
SiO_2	54.97	50.30	51.73	53.34 ± 0.38	55.19 ± 0.61	59.93	64.85
MgO	0.06	11.67	13.42	4.22 ± 0.40	3.90 ± 0.22	1.06	1.58
Al_2O_3	27.66	1.34	1.68	15.18 ± 0.19	15.85 ± 0.40	11.22	11.26
K_2O	0.34	bdl	0.03	0.94 ± 0.39	0.49 ± 0.15	7.07	2.27
CaO	10.88	17.88	14.81	7.22 ± 0.17	8.42 ± 0.57	1.25	0.99
TiO_2	0.06	0.78	0.49	0.90 ± 0.22	0.84 ± 0.08	2.97	3.20
MnO	bdl	0.35	0.40	0.17 ± 0.01	—	—	—
FeO	1.22	17.14	18.53	12.97 ± 0.52	11.74 ± 0.53	16.11	15.14
Cr_2O_3	bdl	0.04	0.02	bdl	—	—	—
NiO	bdl	0.04	bdl	0.02 ± 0.02	—	—	—
Tot.	100.21	99.74	101.33	96.96	100.00	100.00	100.00

Cc = cataclasite; UM = unidentified mineral; avg = average; am.ph = amorphous phase; bdl = below detection limit.

cones, were found. The chemical composition of these features is largely consistent with silica melt, with local variation, as in the Vredefort shatter cones. These features are not similar to those described in this work. On the other hand, the finding in the shatter cones from the Santa Fe structure (Fackelmann et al. 2008) is quite close to those observed in Vista Alegre shatter cones. The authors described a 50 μm thick, cryptocrystalline layer, which seems to be consistent with melt coating the striated surface. The same material apparently occurs also in veinlets that develop subparallel to the striated surface. Unfortunately, this possible melt layer was not investigated in detail and no information is available on the size of the possible Santa Fe impact crater; therefore, a complete comparison between the two structures cannot be made. The description of the melt film found on shatter cone surfaces of the Keurusselkä structure seems similar to our findings, although with a different target material (Hasch et al. 2015). The vesicular melt film found on the surface of experimentally produced shatter cones in sandstone (Kenkmann et al. 2012) is also similar to our observations. Although these recent descriptions are only available in abstract form, there are a few relevant similarities with the findings for the Vista Alegre shatter cones, such as (1) the occurrence of melt rock film that is vesicular, apparently amorphous, and continuous or at least extended over a certain distance; (2) an offset, which suggests a shear component.

Why Not (Hydrothermal) Alteration?

A continuous dark layer on shatter cone surfaces probably has already been noticed in other samples, but was not studied in detail, because it was interpreted as hydrothermal vein or secondary alteration. We suggest that the investigated vein consists of melt for the following reasons.

1. A hydrothermal vein would have crosscut the whole impact breccia in which the shatter cones were found. Although the deposition process of the suevite is still debated, it had filled the crater before hydrothermal circulation was established. Shatter cones were "entrapped" and thus preserved in the breccia. Also, the breccia exhibits no evidence of hydrothermal alteration.
2. The occurrence of sandstone among the clasts in the impact breccia and in blocks in the central area of the crater suggests that hydrothermal fluids would have been enriched in mobile alkali elements and silica. The investigated phases of the studied melt film on shatter cone surfaces do not display any trace of such a chemical signature. Also the trace element composition of shatter cones in the impact breccia shows negligible variation with respect to that of the unshocked basalt (Table 1 in this work and table 1 in Crósta et al. 2010), except for an anomalous enrichment in Cr in our analyses that might be a local contamination; a higher LOI, which is consistent with the weathering of the sample and the occurrence of secondary fractures crosscutting the whole sample; and the presence of sheet minerals (e.g., Fig. 4b).
3. As discussed in detail in the following section, the shape and the chemical composition of the unidentified phase support formation by fast crystallization from a basaltic melt. In addition, amorphous material in the vein (likely glass) and micas (possibly devitrification phases), have been found next to the unidentified phase.

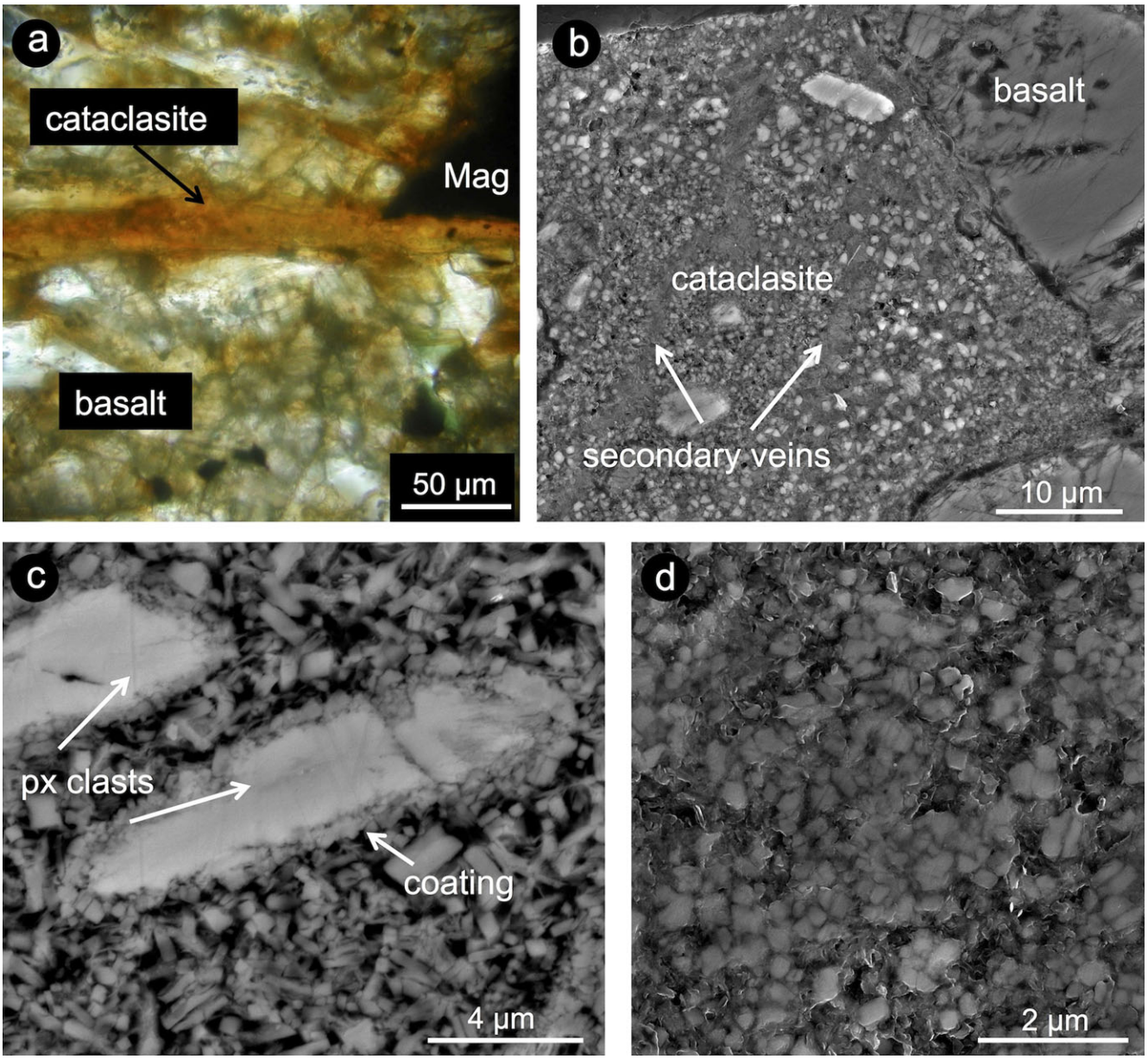

Fig. 4. Cataclastic layers in shatter cones. a) Cataclastic layer (light brown) in unshocked basalt. The magnetite (Mag, black) on the upper right suggests an offset along the cataclasite. Plane-polarized light photograph. b) Detail of the sharp boundary of the cataclasite. BSE-SEM image. c) Pyroxene clasts in the fine-grained matrix of the cataclasite. Notice the subrounded shape of the clasts, which are apparently coated by very fine-grained grains. BSE-SEM image. d) The cataclasite matrix showing evidence of sintering among the grains. BSE-SEM image.

The Crystalline Phase in the Melt Layer

The identification of the crystalline phase that formed in the melt layer might provide constraints on the melt formation and crystallization and, therefore, we put much effort into an attempt to characterize this mineral. In comparison with friction melts, formed along a fault plane during a seismic event, commonly called pseudotachylytes by structural geologists, the finding of a rare phase with specific crystallization conditions can constrain the minimum melt temperature (e.g., Nestola et al. 2010). In that study, the authors found dmisteinbergite, an uncommon polymorph of anorthite in a pseudotachylyte formed in granitoid. This mineral crystallizes during fast cooling of a melt with an anorthitic composition, under specific temperature conditions. The experimental constraints on dmisteinbergite crystallization have allowed these

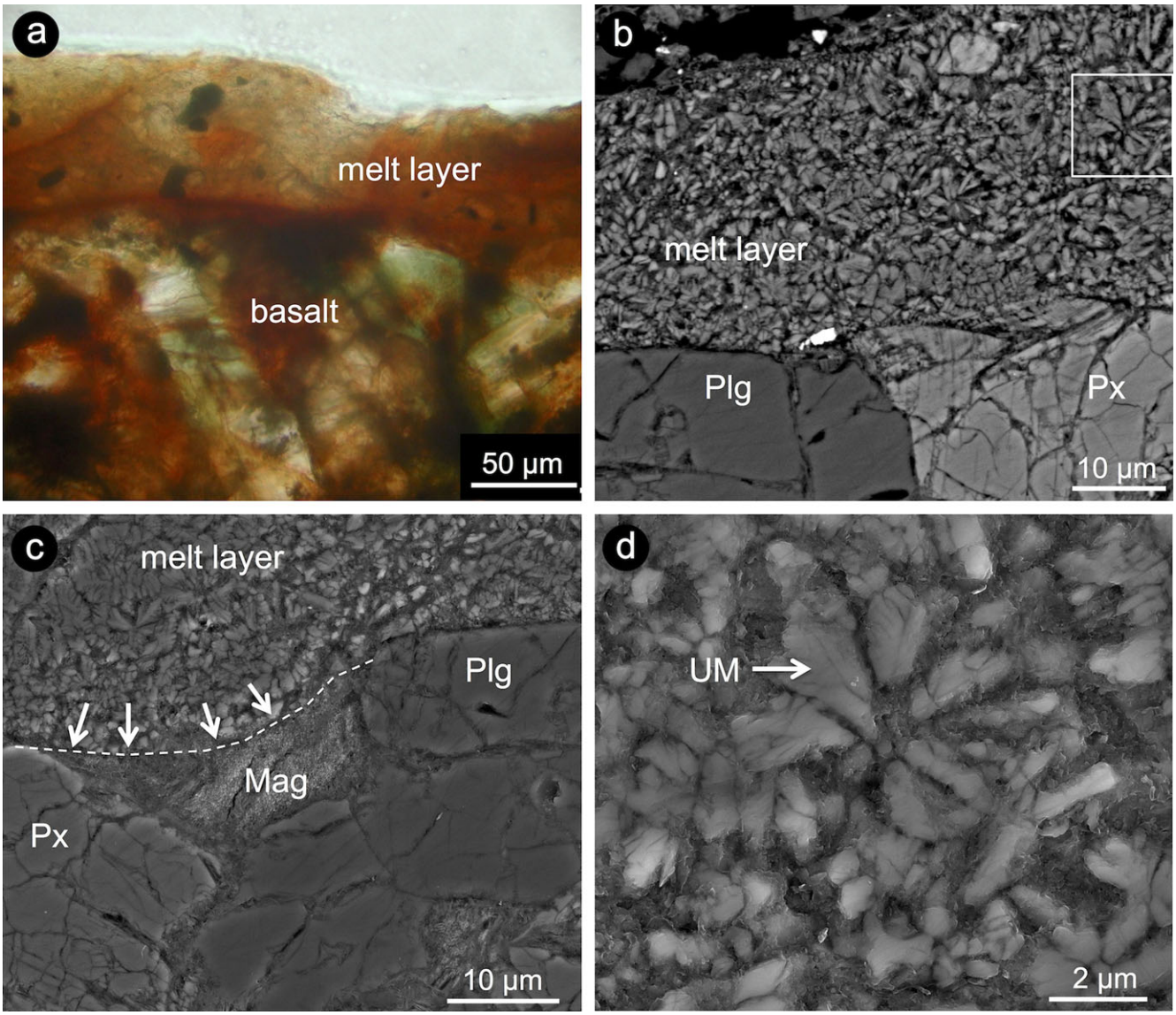

Fig. 5. The melt layer in shatter cones. a) Glassy appearance of the melt layer (reddish) on the striated surface of shatter cones, with a sharp contact with the host basalt. Plane-polarized light photograph. b) Internal fabric of the melt layer. The melt is apparently completely crystallized and has a sharp boundary with the basalt (Plg = plagioclase, Px = pyroxene). BSE-SEM image. c) Effect of thermal breakdown on the magnetite (Mag) but not on plagioclase (Plg) and pyroxene (Px) in the host basalt in contact with the melt layer. The thermal breakdown of magnetite determines also the occurrence of an embayment. BSE-SEM image. d) Detail of the crystalline phases (UM = unidentified mineral) in the melt, showing dendritic growth and the possible occurrence of an amorphous phase. BSE-SEM image.

authors to estimate the melt temperature and the quenching speed of the studied pseudotachylyte. On the surface of shatter cones, quenching from a superheated melt of basaltic composition could have allowed the crystallization of a phase, which might indicate exceptional conditions of formation.

The chemical analyses, although clearly confirming the composition of the crystalline phase, did not lead to unambiguous identification of the phase. The sum of the major components from the microprobe analysis is lower than 100 wt% (Table 2). This is likely caused either by the presence of OH and other volatiles or by a porous structure. A phase with a high content in volatiles would probably have been destabilized and damaged by the well-focused and highly energetic beam of the microprobe and of TEM (see the effect on Si-bearing glasses; e.g., Humphreys et al. 2006). As this did not happen in our sample, a high content of water in the mineral structure can be reasonably excluded. An alternative explanation for the missing elements in the

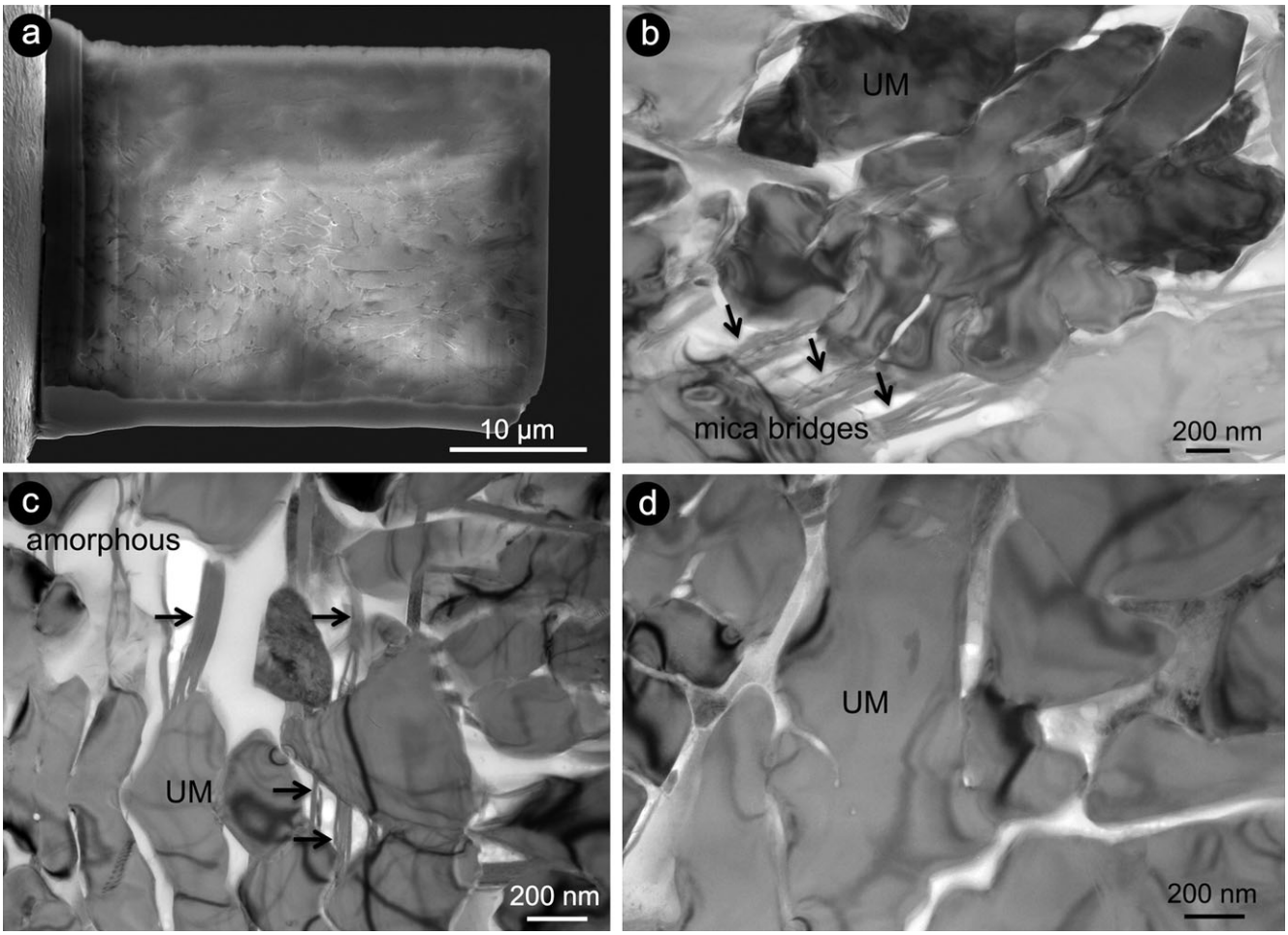

Fig. 6. The unidentified crystalline phase (UM) in the melt layer. a) Foil containing the analyzed phase during the FIB thinning, cut orthogonal to the surface is shown in Fig. 5. The internal fabric of the crystalline aggregate is visible. SE-SEM image. b) TEM image of the unidentified crystalline phase, showing dendritic shape and mica "bridges" between crystals. c) Detail of the aggregate of unidentified crystals with an amorphous phase rimming the grain boundaries and the mica bridges (marked by black arrows). TEM image. d) Detail of the unidentified crystalline phase showing the irregular margin, the absence of structural defects, and the presence of an amorphous phase in the crystal embayments.

budget might be the spatial resolution of the microprobe (interaction volume is about 1 μm^3) in comparison with the grain size of the unidentified phase (nm) and its irregular shape. Some of our microprobe analyses are probably contaminated by the other phases in the melt layer, because of the ultrafine grain size of the investigated phase compared with the interaction volume of the beam, and for this reason were not considered in this work. With the TEM, the microfabric of the melt vein has been resolved: there are crystals with dendritic shapes, connected by sheet minerals, and an amorphous phase occurs as well. The characteristics of the TEM beam ensure high-resolution EDX analyses. Although EDX provides only semiquantitative analyses and the measurements are automatically normalized to 100 wt%, the resulting composition of the crystalline phase is consistent with that obtained by microprobe (Table 2), and no other peaks, which might indicate missing elements, were observed in the spectrum. This excludes significant contamination of the selected microprobe analyses of the unidentified phase from the other phases in the melt layer. The chemical analysis of the unidentified phase shows major element contents that are close to those of the bulk basalt (Table 1) and in between that of plagioclase and pyroxene (Table 2). An attempt to calculate the mineral stoichiometry, assuming 6 atoms of oxygen, yielded the formula $(Na_{0.25}\ Ca_{0.32}\ K_{0.02})(Mg_{0.21}\ Al_{0.64}\ Fe_{0.35}\ Ti_{0.02})(Si_{1.97}\ Al_{0.03})O_6$. This formula does not correspond to any reasonable candidate. Possible contamination by mica is very unlikely because of the high analytical resolution of the instrument and because this mineral has a very

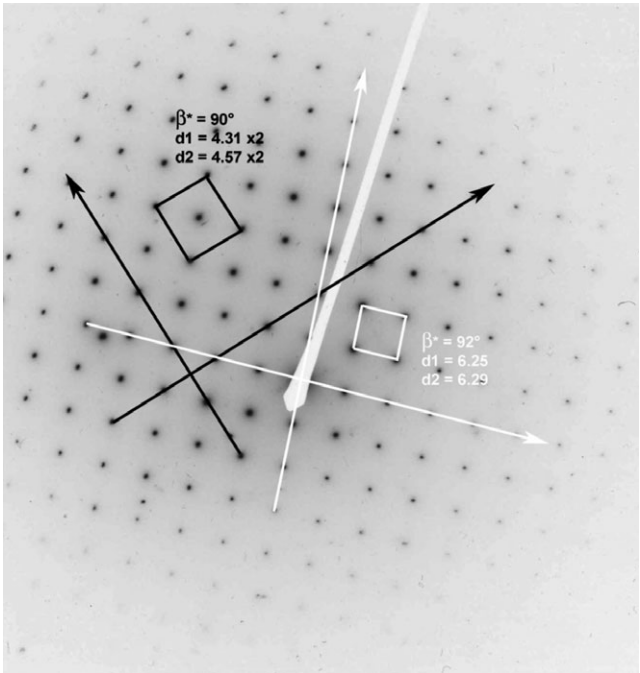

Fig. 7. Diffraction pattern of the unidentified phase, with two possible cell parameters.

different elemental composition. A possible intergrowth of different phases can be excluded because the diffraction pattern (Fig. 7) and the TEM images (Fig. 6) clearly point to a single mineral structure. The data on the amorphous phase indicate that this is most likely a preserved glass. Notably, the amorphous material is enriched in Si and Ti with respect to both the unidentified phase and the mica. The stoichiometry of the mica does not fit this phase well, but the EDX analyses are not completely trustworthy, especially for the quantification of K. All this information suggests that the crystalline phase grew from a melt of basaltic composition, consistent with the basalt in which the shatter cones were formed.

Characterization of the crystalline phase has been attempted using Raman spectroscopy (Fig. 8) and TEM. The ultrafine grain size of the investigated crystals in comparison with the spatial resolution of the Raman spectrometer probably resulted in contamination from other phases in the melt layer. In addition, the incomplete removal of the carbon coating and of other organic material from the irregular surface of the melt layer has resulted in high fluorescence that has reduced the quality of the analysis. The obtained spectra for the unidentified phases show weak peaks, reminiscent of those typical for a pyroxene (Fig. 8), but with a wavelength shift out of the range commonly related to pyroxene (for the three major peaks, the range is approximately 312–343 cm^{-1}, 660–685 cm^{-1}, and 990–1011 cm^{-1}; after the online Rruff database, Downs 2006). The estimate of the cell size of the crystalline phase, as obtained by electron diffraction, seems to fit with pigeonite (as suggested by Wirth, personal communication), but the amount of Ca detected in the phase is much higher than that admitted in pigeonite, even under extreme conditions (e.g., Domeneghetti et al. 2005; Alvaro et al. 2011). In addition, the octahedral site cannot be completely filled. Nevertheless, the hypothesis of a monoclinic pyroxene is the most likely one, although the chemical composition does not fit any known pyroxene. Further TEM analyses, including electron diffraction tomography, will have to be performed to completely characterize this uncommon phase.

The shape of the nanocrystals is similar to that of microlites, which crystallize in melts (e.g., Ross 1962). Microlites are known in volcanic environments (e.g., Sharp et al. 1996) but also in friction- (e.g., Magloughlin and Spray 1992; Di Toro and Pennacchioni 2004) and shock-induced melts (e.g., Pittarello and Koeberl 2013). In the investigated case, the unidentified phase has a dendritic shape with irregular margins, suggesting fast crystallization under disequilibrium conditions. This supports the origin of the unidentified phase by quenching from a melt.

Melt Formation on Shatter Cone Surfaces

Although the crystalline phase was not identified and the melt temperature is therefore unconstrained, the occurrence of this phase supports the existence of a melt film, at least locally, on shatter cones' surfaces. Unfortunately only limited information on the 3-D distribution of this melt film is available because observations were made on a sample that occurs as a clast in the breccia and because the thin section was cut normal to the shatter cone surfaces and parallel to the striation. Although laterally limited, the observations with the optical microscope and the SEM support the hypothesis of a roughly continuous melt film, with a generally constant thickness, located along the striations (likely in a groove). The occurrence of a continuous melt film on the surfaces of shatter cones and the presence of ultracataclasites with similar features to the melt film that occur subparallel to the striated surface of shatter cones suggests that the formation of both the melt film and of the cataclasites is related to the formation of the shatter cones at Vista Alegre. Thus, a formation mechanism that explains the striations, the comminution, and the melting has to be found.

Shatter cones in Vista Alegre are mostly found in impact breccia, likely suevite. Therefore, shatter cones must have formed during the early stages of the impact

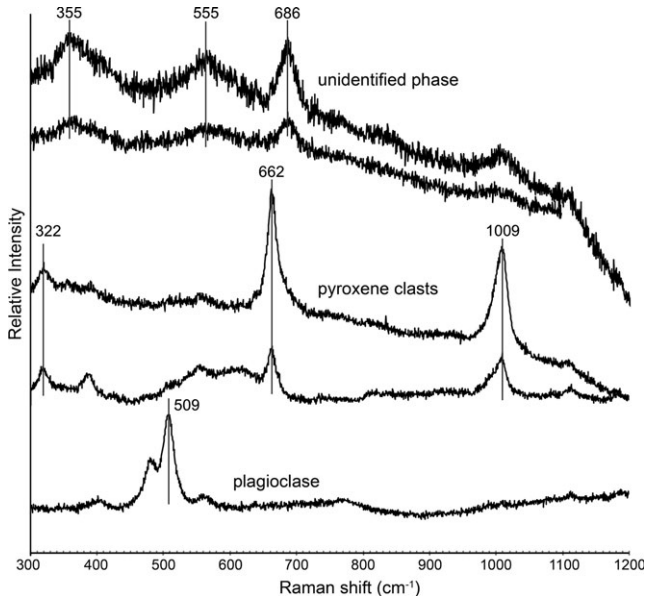

Fig. 8. Raman spectra of unidentified phase, in comparison with that of pyroxene in clasts in a cataclastic layer and plagioclase in the wall rock. The Raman intensity is relative and has been exaggerated for the unidentified phase. The wavelengths of the most prominent peaks are indicated.

event. We discuss here three hypotheses of melt generation on shatter cone surfaces, according to our findings on the Vista Alegre shatter cones.

Maximum Shear Stress (Shock Compression)

According to Dawson (2009), melt on shatter cone surfaces forms along planes that experience the maximum shear stress during shock compression. Localized high strain rates can trigger melting and therefore lubrication of the surface, dramatically reducing the shear strength of the rock (e.g., Di Toro et al. 2006). A similar process can be considered here for shock compression. This would be consistent with the formation of shatter cones in the early stage of crater formation and explain the finding of shatter cones as clasts in a suevitic breccia. The model predicts straight conical surfaces but this is in contrast to the spoon-shaped shatter cones observed in nature (e.g., Baratoux et al. 2014; Sagy et al. 2004). In the investigated sample, striations have been found on opposite surfaces and with opposite orientation, but according to the model this can be explained by a wide shock front. Unfortunately the limited size of the sample and its occurrence as a clast in a breccia hampers a full 3-D view and the original orientation of the shatter cone. The extreme localization of the thin melt film observed in Vista Alegre shatter cones might be consistent with this model. On the other hand, this mechanism, under the shock compression regime, is not likely to produce fine-grained cataclasites such as those observed, which recalls fault gauges for their ultrafine grain size. Furthermore, this model does not predict any offset and parallel (cone-in-cone) structure.

Frictional Heating

Along a slip plane, under certain conditions, the heating induced by friction between the asperities can cause melting (e.g., Spray 2010). Gibson and Spray (1998) have claimed that symmetric slip could have occurred on shatter cone surfaces, to justify the limited or absent offset observed at shatter cone surface. Indeed in Vista Alegre shatter cones, a minor offset has been observed in the cataclasites (Fig. 4a). The formation of a cataclasite by crushing grains along a "fault" might be consistent with the hypothesis of frictional heating (for comparison with seismic faults: Curewitz and Karson 1999; Hadizadeh and Johnson 2003; Craddock and Magloughlin 2005). Other similarities with friction products are the occurrence of microlites in the melt, the thermal breakdown of magnetite at the margin, the preferred orientation of clasts in the cataclasite, and the sharp margins of the melt layer and the cataclasite with the host rock. In contrast to the hypothesis of frictional formation, the melt layer lacks injection veins, which are fractures, almost normal to the shear plane, filled with melt. In addition, if this process had occurred along a tectonic fault, the slip required to produce a 50 μm thick melt layer should be at least 12 cm (in Pittarello et al. 2008; a paleoseismic fault has been investigated, with 1.44 m of displacement and an average thickness of the pseudotachylyte of 0.6 mm). Experimental work by Kenkmann et al. (2000) showed that friction is an important source of heating for the generation of melt even in the case of shock. In the experiments by Kenkmann et al. (2000), the ratio displacement/thickness necessary to produce a melt vein is still very high, consistent with our first-order calculation. Considering only the possibility of symmetric slip induced by shock waves along the surface of shatter cones, the melt layer and the cataclasites observed in Vista Alegre shatter cones might be consistent with the hypothesis of frictional heating. In this case, the timing of the melt formation during the impact event is unclear.

Adiabatic Decompression

Wieland et al. (2006) described subparallel sets of fractures that they ascribe to a tensile regime. These authors, therefore, suggested that these fractures, the striations on shatter cones, and the melt are all produced by shock unloading after passage of the trail of shock waves through the rock. These authors explain

the minor displacements observed along some fractures as a minimum contribution from frictional melting. The cataclasites that are subparallel to the striated surface of shatter cones from Vista Alegre are similar to the subparallel sets of fractures (called "multiple striated joint sets") described by Nicolaysen and Reimold (1999) and Wieland et al. (2006) from the Vredefort structure, and their occurrence is therefore consistent with the assumed tensile fracturing. In addition, this model predicts a localized effect, not affecting the rest of the rock of the shatter cone.

Except for Dawson (2009), there is general agreement regarding shatter cone formation: it involves tensile fracturing at the tail of fast propagating shock waves and the occurrence of heterogeneities is required for nucleating conical shape fractures (Sagy et al. 2002, 2004; Baratoux and Melosh 2003; Wieland et al. 2006; Kenkmann et al. 2012; Wilk and Kenkmann 2015). The finding of a melt film in experimentally produced shatter cones is interpreted as evidence of a shear component by Wilk and Kenkmann (2015), and in natural samples a small offset is locally observed (Wieland et al. 2006).

The cataclasite observed in Vista Alegre shatter cones closely resembles a fault gouge. Tensile stress at the tip of a fast propagating shear fracture (close to Rayleigh wave velocity) has been invoked for gouge formation during a seismic event, rather than extreme comminution by prolonged slip (Reches and Dewers 2005). The thickness of the damaged zone and the deformation intensity are likely related to the propagation velocity and both decrease quickly with the distance from the tip. In the case of shock, the propagation velocity might be even faster than during an earthquake, which also explains the melting of pulverized rock. These principles were also invoked by Sagy et al. (2002, 2004) in their model of shatter cone formation. If shatter cones formed by tensile fracturing at the tip of the fast propagating rupture, the process can occur during the early stages of the impact event, triggered by the tensile stress at the tail of the shock front of the first trail of shock waves emanated at the contact stage of impact cratering.

CONCLUSIONS

In the Vista Alegre impact structure, shatter cones have formed in fine-grained basalt and have been found as clasts in suevitic impact breccia. In one shatter cone sample, which exhibits striations on opposite surfaces, thin ultracataclasites and a melt film have developed subparallel to and on striated surfaces. The melt film mostly consists of a dendritic crystalline phase, which has a composition close to that of the bulk basalt, mica, and an amorphous phase. The crystalline phase, although not yet identified, shows characteristics that point to a formation by quenching of a melt of basaltic composition. The cataclastic layers occur subparallel to the melt decorated surfaces, and contain subrounded clasts of pyroxene in an ultrafine-grained matrix with a possible offset. Combining observations from paleoseismic faults, which have similar features to those described here, and the models proposed for shatter cone formation, cataclasites and melt films on a striated surface are likely consistent with shock-induced tensile fracturing by fast propagation of the tip of the rupture. Tensile stress is expected at the tail of the first shock compressional pulse. Thus, the formation of shatter cones and the related features observed in the Vista Alegre samples are consistent with the general model of shatter cones formed during the early stages of crater formation, which also explains their occurrence as clasts in the suevitic breccia.

Acknowledgments—G. Habler, F. Kiraly, and D. Mader of the Department of Lithospheric Research of the University of Vienna, Austria are thanked for their technical assistance at the SEM-FIB, EMPA, and INAA respectively. K. Baert is thanked for Raman spectroscopy at the SURF Department of the Vrije Universiteit Brussel, Brussels, Belgium. LP was supported by the Austrian FWF, project P21821-N19. S. McKibbin is thanked for language check. We thank R. Wirth, D. Baratoux, T. Kenkmann, and M. Poelchau for constructive reviews and insightful comments on the manuscript. M. Poelchau is also thanked for the editorial handling.

Editorial Handling—Dr. Michael Poelchau

REFERENCES

Alvaro M., Cámara F., Domeneghetti M. C., Nestola F., and Tazzoli V. 2011. HT $P2_1/c$–$C2/c$ phase transition and kinetics of Fe^{2+}–Mg order–disorder of an Fe-poor pigeonite: Implications for the cooling history of ureilites. *Contributions to Mineralogy and Petrology* 162:599–613.

Baratoux D. and Melosh H. J. 2003. The formation of shatter cones by shock wave interference during impacting. *Earth and Planetary Science Letters* 216:43–54.

Baratoux D., Bouley S., Reimold W. U., and Baratoux L. 2014. The first three dimensional models of shatter cones (abstract #5020). *Meteoritics & Planetary Science* 49:A50.

Craddock J. P. and Magloughlin J. F. 2005. Calcite strains, kinematic indicators, and magnetic flow fabric of a Proterozoic pseudotachylyte swarm, Minnesota River Valley, USA. *Tectonophysics* 402:153–168.

Crósta A. P., Kazzuo-Vieira C., and Schrank A. 2004. Vista Alegre: A newly discovered impact crater in southern Brazil (abstract). *Meteoritics & Planetary Science* 39:A28.

Crósta A. P., Koeberl C., Furuie R., and Kazzuo-Vieira C. 2010. The first description and confirmation of the Vista Alegre impact structure in the Paraná flood basalts of southern Brazil. *Meteoritics & Planetary Science* 45:181–194.

Crósta A. P., Jourdan F., and Koeberl C. 2012. $^{40}Ar/^{39}Ar$ dating of the Vista Alegre impact crater, Brazil (abstract #2733). 34th International Geological Congress, Brisbane.

Curewitz D. and Karson J. A. 1999. Ultracataclasis, sintering, and frictional melting in pseudotachylytes from East Greenland. *Journal of Structural Geology* 21:1693–1713.

Dawson E. 2009. Meteorite impact shatter cones—Adiabatic shear bands? DYMAT 2009: 9th International Conference on the Mechanical and Physical Behavior of Materials under Dynamic Loading, Brussels—Belgium, 7–11 September 2009, Vol. 2, pp. 1471–1477.

Dietz R. S. 1947. Meteorite impact suggested by the orientation of shatter-cones at the Kentland, Indiana, disturbance. *Science* 105:42–43.

Dietz R. S. 1960. Meteorite impact suggested by shatter cones in rock. *Science* 131:1781–1784.

Di Toro G. and Pennacchioni G. 2004. Superheated friction-induced melts in zoned pseudotachylytes within the Adamello tonalites (Italian Southern Alps). *Journal of Structural Geology* 26:1783–1801.

Di Toro G., Hirose T., Nielsen S., Pennacchioni G., and Shimamoto T. 2006. Natural and experimental evidence of melt lubrication of faults during earthquakes. *Science* 311:647–649.

Domeneghetti M. C., Zema M., and Tazzoli V. 2005. Kinetics of Fe^{2+}-Mg order-disorder in $P2_1/c$ pigeonite. *American Mineralogist* 90:1816–1823.

Downs R. T. 2006. The RRUFF Project: An integrated study of the chemistry, crystallography, Raman and infrared spectroscopy of minerals. Program and Abstracts of the 19th General Meeting of the International Mineralogical Association in Kobe, Japan. O03-13.

Fackelmann S. P., Morrow J. R., Koeberl C., and McElvain T. H. 2008. Shatter cone and microscopic shock-alteration evidence for a post-Paleoproterozoic terrestrial impact structure near Santa Fe, New Mexico, USA. *Earth and Planetary Science Letters* 270:290–299.

Ferriere L. and Osinski G. R. 2010. Shatter cones and associated shock-induced microdeformations in minerals—New investigations and implications for their formation (abstract #1392). 41st Lunar and Planetary Science Conference. CD-ROM.

Ferriere L., Raiskila S., Osinski G. R., Pesonen L. J., and Lehtinen M. 2010. The Keurusselkä impact structure, Finland—Impact origin confirmed by characterization of planar deformation features in quartz grains. *Meteoritics & Planetary Science* 45:434–446.

French B. M. and Koeberl C. 2010. The convincing identification of terrestrial meteorite impact structures: What works, what doesn't, and why. *Earth-Science Reviews* 98:123–170.

Gay N. C. 1976. Spherules on shatter cone surfaces from the Vredefort Structure, South Africa. *Science* 194:724–725.

Gay N. C., Comins N. R., and Simpson C. 1978. The composition of spherules and other features in shatter cone surfaces from the Vredefort structure, South Africa. *Earth and Planetary Science Letters* 41:372–380.

Gibson H. M. and Spray J. G. 1998. Shock-induced melting and vaporization of shatter cone surfaces: Evidence from the Sudbury impact structure. *Meteoritics & Planetary Science* 33:329–336.

Govindaraju K. 1989. Compilation of working values and sample description for 272 geostandards. *Geostandards Newsletter* 13:1–113.

Hadizadeh J. and Johnson W. K. 2003. Estimating local strain due to comminution in experimental cataclastic textures. *Journal of Structural Geology* 25:1973–1979.

Hargraves R. B. and White J. C. 1996. Micro-shock deformation adjacent to the surface of shatter cones from the Beaverhead impact structure, Montana. *The Journal of Geology* 104:233–238.

Hasch M., Reimold W. U., Zaag P. T., Raschke U., Hobson K., and Hess K. U. 2015. Shatter cones at the Keurusselkä impact structure and their relation to local jointing (abstract #1376). 46th Lunar and Planetary Science Conference. CD-ROM.

Humphreys M. C. S., Kearns S. L., and Blundy J. D. 2006. SIMS investigation of electron-beam damage to hydrous, rhyolitic glasses: Implications for melt inclusion analysis. *American Mineralogist* 91:667–679.

Jarosewich E., Clarke R. S. J., and Barrows J. N. 1987. The Allende meteorite reference sample. *Smithsonian Contributions to the Earth Sciences* 27:1–49.

Kenkmann T., Hornemann U., and Stöffler D. 2000. Experimental generation of shock-induced pseudotachylites along lithological interfaces. *Meteoritics & Planetary Science* 35:1275–1290.

Kenkmann T., Poelchau M. H., Trullenque G., Hoerth T., Schäfer F., Thoma K., and Deutsch A. 2012. Shatter cones formed in a MEMIN impact cratering experiment (abstract #5092). 75th Annual Meteoritical Society Meeting.

Koeberl C. 1993. Instrumental neutron activation analysis of geochemical and cosmochemical samples: A fast and proven method for small sample analysis. *Journal of Radioanalytical and Nuclear Chemistry* 168:47–50.

Mader D. and Koeberl C. 2009. Using instrumental neutron activation analysis for geochemical analyses of terrestrial impact structures: Current analytical procedures at the University of Vienna Geochemistry Activation Analysis Laboratory. *Applied Radiation and Isotopes* 67:2100–2103.

Magloughlin J. F. and Spray J. G. 1992. Frictional melting processes and products in geological materials: Introduction and discussion. *Tectonophysics* 204:197–206.

Martini J. E. J. 1991. The nature, distribution and genesis of the coesite and stishovite associated with the pseudotachylite of the Vredefort Dome, South Africa. *Earth and Planetary Science Letters* 103:285–300.

Nestola F., Mittempergher S., Di Toro G., Zorzi F., and Pedron D. 2010. Evidence of dmisteinbergite (hexagonal form of $CaAl_2Si_2O_8$) in pseudotachylyte: A tool to constrain the thermal history of a seismic event. *American Mineralogist* 95:405–409.

Nicolaysen L. O. and Reimold W. U. 1999. Vredefort shatter cones revisited. *Journal of Geophysical Research* 104:4911–4930.

Pittarello L. and Koeberl C. 2013. Petrography of impact glasses and melt breccias from the El'gygytgyn impact structure, Russia. *Meteoritics & Planetary Science* 48:1236–1250.

Pittarello L., Di Toro G., Bizzarri A., Pennacchioni G., Hadizadeh J., and Cocco M. 2008. Energy partitioning during seismic slip in pseudotachylyte-bearing faults (Gole

Larghe Fault, Adamello, Italy). *Earth and Planetary Science Letters* 269:131–139.

Reches Z. and Dewers T. A. 2005. Gouge formation by dynamic pulverization during earthquake rupture. *Earth and Planetary Science Letters* 235:361–374.

Reimold W. U., Koeberl C., and Bishop J. 1994. Roter Kamm impact crater, Namibia: Geochemistry of basement rocks and breccias. *Geochimica et Cosmochimica Acta* 58:2689–2710.

Ross C. S. 1962. Microlites in glassy volcanic rocks. *American Mineralogist* 47:723–740.

Sagy A., Reches Z., and Fineberg J. 2002. Dynamic fracture by large extraterrestrial impacts as the origin of shatter cones. *Nature* 418:310–313.

Sagy A., Fineberg J., and Reches Z. 2004. Shatter cones: Branched, rapid fractures formed by shock impact. *Journal of Geophysical Research* 109:B10209. doi:10.1029/2004JB003016.

Schneider B. and Wagner G. A. 1976. Shatter cones produced experimentally by impacts in limestone targets. *Earth and Planetary Science Letters* 32:40–44.

Sharp T. G., Stevenson R. G., and Dingwell D. B. 1996. Microlites and "nanolites" in rhyolitic glass: Microstructural and chemical characterization. *Bulletin of Volcanology* 57:631–640.

Spray J. G. 2010. Frictional melting processes in planetary materials: From hypervelocity impact to earthquakes. *Annual Review of Earth and Planetary Sciences* 38:221–254.

Stöffler D. and Grieve R. A. F. 2007. Impactites. In: *Metamorphic rocks: A classification and glossary of terms, recommendations of the International Union of Geological Sciences*, edited by Fettes D. and Desmons J. Cambridge, UK: Cambridge University Press. pp. 82–92, 111–125, and 126–242.

Vasconcelos M. A. R., Crósta A. P., Reimold W. U., Góes A. M., Kenkmann T., and Poelchau M. H. 2013. The Serra da Cangalha impact structure, Brazil: Geological, stratigraphic and petrographic aspects of a recently confirmed impact structure. *Journal of South American Earth Sciences* 45:316–330.

Wieland F., Reimold W. U., and Gibson R. L. 2006. New observations on shatter cones in the Vredefort impact structure, South Africa, and evaluation of current hypotheses for shatter cone formation. *Meteoritics & Planetary Science* 41:1737–1759.

Wilk J. and Kenkmann T. 2015. The surface structure of shatter cones in experimental impact craters (abstract #2637). 46th Lunar and Planetary Science Conference. CD-ROM.